The Production of Ti-W alloys from Mixed Oxide Precursors via the FFC Cambridge Process

R. Bhagat, M. Jackson, D. Inman, R. Dashwood

Abstract

Ti-10 wt. % W alloys were produced via the electrochemical deoxidation of mixed TiO_2+WO_3 sintered precursors in a molten $CaCl_2$ electrolyte at 1173 K. The reduction of these ceramic precursors was characterised by analysing several partially reduced samples taken periodically through the deoxidation process. Fully metallic samples were retrieved after 15 h of reduction. This reduction time was longer than that observed by the authors for metallisation of $(Ti,Mo)O_2$ sintered precursors. This was believed to occur as a result of significant differences in the reduction pathway, despite tungsten and molybdenum possessing similar interactions with titanium (group VI elements). It was found that reduction initiated with the rapid reduction of WO_3 to a W-Ti particulate. TiO_2 then proceeded to reduce sequentially through the lower oxides, with the formation of $Ca(Ti,W)O_3$. Between 1 h and 3 h of reduction the sample is believed to be composed of $Ca(Ti,W)O_3$ and TiO. A comproportion reaction between the two phases is then observed with the formation of W-Ti and $CaTi_2O_4$, which then proceeds to reduce to titanium. However homogenisation between the product titanium and W-Ti does not take place until the titanium is sufficiently deoxidised, thus β Ti forms late in the reduction process. It is believed that the lack of formation of β Ti early on in the reduction process, coupled with the lack of formation of a conductive (Ti,Mo)O network, accounts for the relatively slow reduction time.

Introduction

The production of beta titanium alloys via conventional methods is an arduous process requiring multiple stages of processing. These alloys are conventionally produced by melting titanium sponge with alloying additions or master alloys. The titanium sponge is produced via the Kroll process [1], a pyro-metallurigical process involving the chlorination of rutile to form $TiCl_4$, which is subsequently reacted with magnesium to form titanium sponge. This process typically requires between eight days and two weeks to produce several tonnes of titanium sponge from rutile. Segregation effects are prominent in these titanium systems, as the alloying additions have a large difference in density and melting point to titanium, thus conventional processing involves several remelts. Alloying tungsten (density 19.25 g cm^{-3}, melting point 3695 K) with titanium (density 4.507 g cm^{-3}, melting point 1941 K) is an example of a system where extremely sluggish diffusion kinetics of tungsten in titanium in addition to the segregation effects make liquid melt processing not viable.

It has been suggested that a likely application for a Ti-W alloy would be as an orthopaedic implant material [ref]. For this application, alloying additions must be carefully selected, as elemental loss due to diffusion can have detrimental effects to the body [ref]. For example, the release of aluminium and vanadium ions from Ti-6Al-4V implants are known to have carcinogenic effects [2, 3]. Despite tungsten not possessing the best biocompatibility, the rate at which it diffuses from titanium is extremely slow. Thus the sluggish kinetics of tungsten in titanium while undesirable from an alloying perspective are favourable from a biocompatibility perspective.

Choe *et al.* [4] produced a number of Ti-10W composites by cold-isostatic pressing titanium and tungsten powders into a perform, prior to hot isostatic pressing for 2 h at 900°C and 100 MPa. These experiments showed that increased levels of tungsten in solid solution produced a complimentary increase in strength and hardness and a lowering of the elastic modulus, which is advantageous for orthopaedic applications. However the presence of interstitial impurities such as oxygen, which can significantly affect the mechanical properties of titanium was not quantified or considered.

The FFC Cambridge process has been used to produce several Ti based alloys systems via the reduction of mixed metal oxides. There has been work published on the Fe-Ti, Ni-Ti and Ti-Mo systems; Ma *et al.* [5] reduced 2 g pellets of natural and synthetic ilmenite ($FeTiO_3$) to FeTi in 4 h, however the pellets were encased in a molybdenum mesh, effectively increasing the electro-active area of the pellet which accounts for the short reduction time. Zhu *et al.* [6] reduced NiO-TiO_2 sintered precursors to form Ni-Ti with low quantities of Ni_3Ti in 8 h. The authors reduced $(Ti,Mo)O_2$ sintered precursors to Ti-15Mo alloy in 9 h [7].

The authors have previously shown that the reduction of reduced TiO_2+WO_3 precursors to form Ti-10W alloy is possible [8]. However, the reduction pathway was not fully investigated. This paper will document the electrochemical formation of homogeneous Ti-10W, by analysing several partially reduced precursors.

Experimental

To form the TiO_2+WO_3 precursors, reagent grade TiO_2 (99.5% Alfa Aesar) and WO_3 (99.998% Alfa Aesar) were combined and ball milled with ethanol and zirconia spheres for 24 hours. The slurry was dried and the powder ground in a mortar and pestle with small quantities of distilled water, which acts as a binding agent. One gram of powder was placed in a 13 mm diameter die prior to uniaxial compaction at 100 MPa. The precursors were then drilled to accept the CP-Ti cathodic current collector and placed on an alumina firing trough and into a furnace. The

precursors were heated at a rate of 3 K min^{-1} and sintered in argon (BOC pureshield – 150 mL min^{-1}) at 1373 K for 3 h.

The electrochemical experiments described in this paper were performed in an Inconel® reaction vessel (SFL Instron) housed in a programmable tube furnace (SFL Instron). Dehydrated calcium chloride ($CaCl_2$) granules (Fluka) were contained in a CP-Ti crucible and thermally equilibrated at 373 K. The $CaCl_2$ salt was then heated to 573 K at 0.1 K min^{-1} under argon (BOC pureshield – 200 mL min^{-1}). The salt was held at this temperature for 5 h prior to being heated to reaction temperature at a rate of 3 K min^{-1}. Prior to reduction the electrolyte was pre-electrolysed for 1 - 3 h to remove electro-active impurities, this was achieved by polarising a grade 2 CP-Ti rod (3 mm Ø) versus a graphite rod (10 mm Ø – Tokai Carbon EC4) to -2700 mV vs. the standard chlorine electrode (S.Cl.E).

The sintered TiO_2-WO_3 precursor was attached to the current collector and suspended above the electrolyte prior to pre-electrolysis. Following the pre-electrolysis, the precursor was lowered into the electrolyte in-circuit and polarised to -500 mV vs. the Ni / $NiCl_2$ reference electrode for 600 s, prior to polarization at a rate of -0.5 mV s^{-1}. These reduction conditions were used to avoid exceeding the upper current limit (1 A) of the potentiostat (Princeton applied research scanning potentiostat model 362). The arrangement of the electrodes and apparatus is shown in Figure 1.

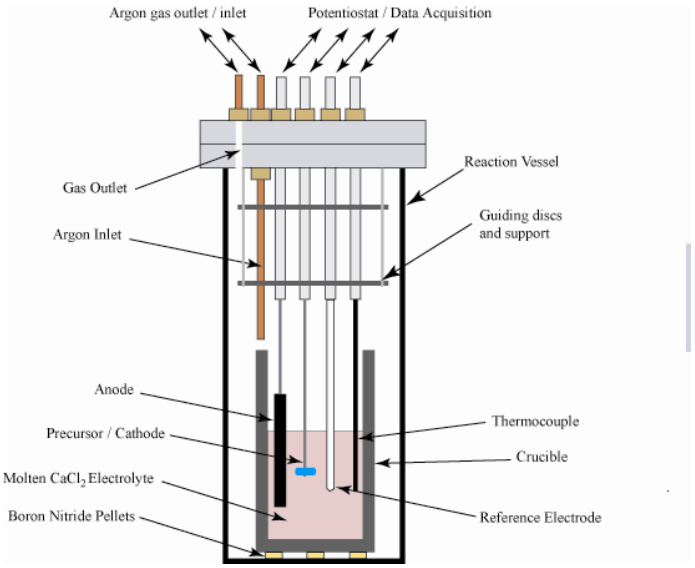

Figure 1 Schematic of the FFC Cambridge reduction cell

Following reduction, samples were ultrasonically cleaned with distilled water to remove residual entrained electrolyte and prepared for analysis using standard metallographic techniques. The samples were characterised by X-ray energy dispersive spectroscopy (X-EDS) and backscattered electron imaging (BEI) using a field emission

gun scanning electron microscope (LEO-FEGSEM) operated at 20.0 keV. X-ray diffraction (XRD) traces were obtained using a Phillips PW 1710 diffractometer using α-Cu radiation and a Ni filter. Phases were identified using indexing information obtained from the EPSRC chemical database services.

Results and Discussion

WO_3 has a range of Magnéli phases similar to that of TiO_2, as such WO_3 can accommodate large concentrations of oxygen vacancies. The intercalation of oxygen vacancies in the WO_3 host lattice produces an effect known as electrochromic colouration resulting in the various Magnéli phases possessing different colours. While stoichiometric WO_3 appears yellow, the Magnéli phases (W_nO_{3n-1} seen in Figure 2) W_5O_{14} and W_4O_{11} appear blue and purple respectively [9].

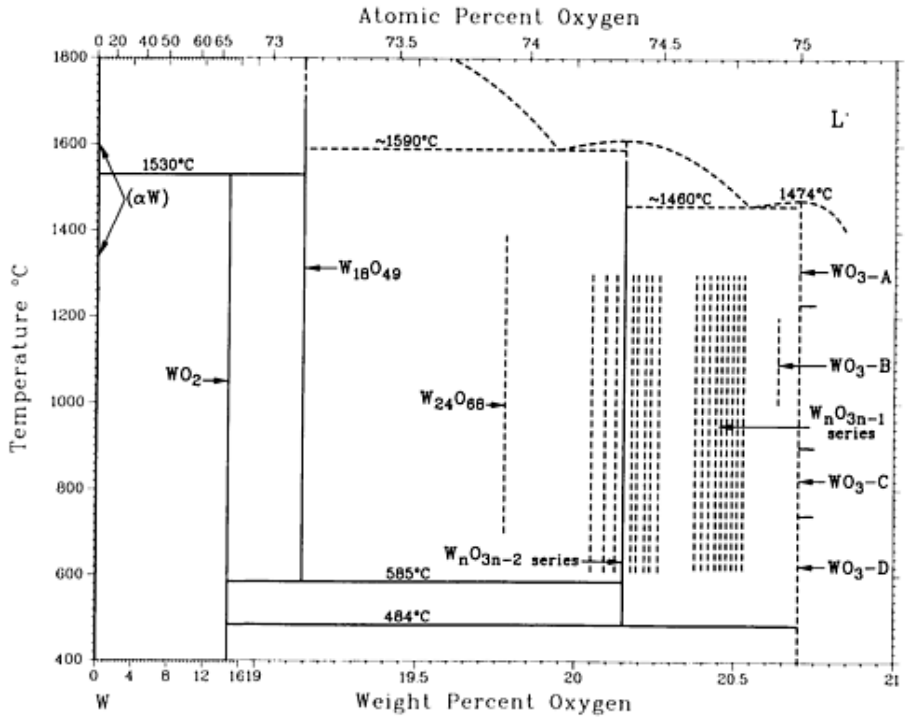

Figure 2 W-O equilibrium phase diagram (redrawn from Wriedt [10])

The as-received tungsten trioxide powder was green in appearance, indicating a mixture of WO_3 and W_5O_{14}, and as such, the unsintered TiO_2-WO_3 precursors were also green. Sintering the precursors in air produced a yellow sintered precursor, indicating the domination of the stoichiometric WO_3 phase. While sintering the precursor under argon produced a deep purple / blue sintered precursor, indicating that a majority of the tungsten trioxide exists as a mixture of W_5O_{14} and W_4O_{11}. Incorporation of oxygen vacancies into the lattice will lead to an increase in the electronic conductivity of tungsten trioxide, thus W_5O_{14} and W_4O_{11} were preferred to stoichiometric WO_3; thus the precursors were sintered in argon. The XRD trace of the sintered precursor (Figure 3a) reveals the presence of

TiO_2, which is expected as the volume fraction of WO_3 present is smaller than can be detected experimentally. The BEI of the sintered precursor (Figure 4a) shows a good distribution of WO_3 and TiO_2 that remain as discreet phases, which is predicted by the TiO_2-WO_3 phase diagram (Figure 5).

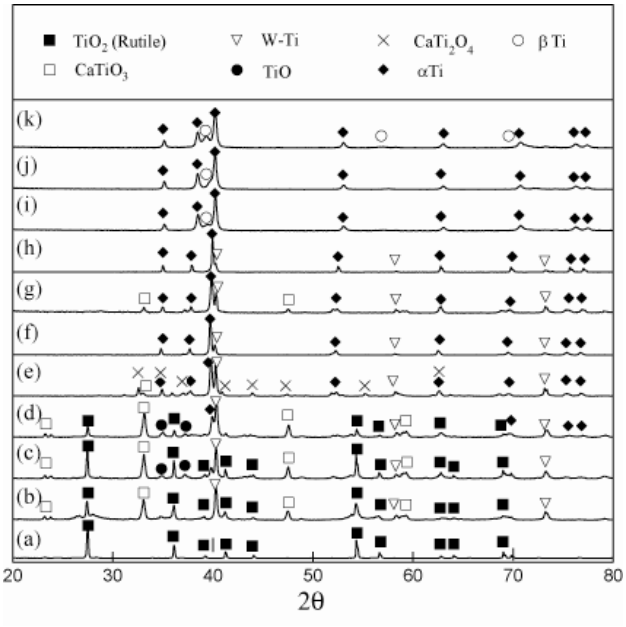

Figure 3 XRD traces for the (a) sintered precursor and partial reductions (b) exposed to electrolyte for 600 s, (c) 1 h, (d) 3 h, (e) 6 h core (f) 6 h edge (g) 9 h core, (h) 9 h edge (i) 15 h, (j) 20 h and (k) 30 h of reduction

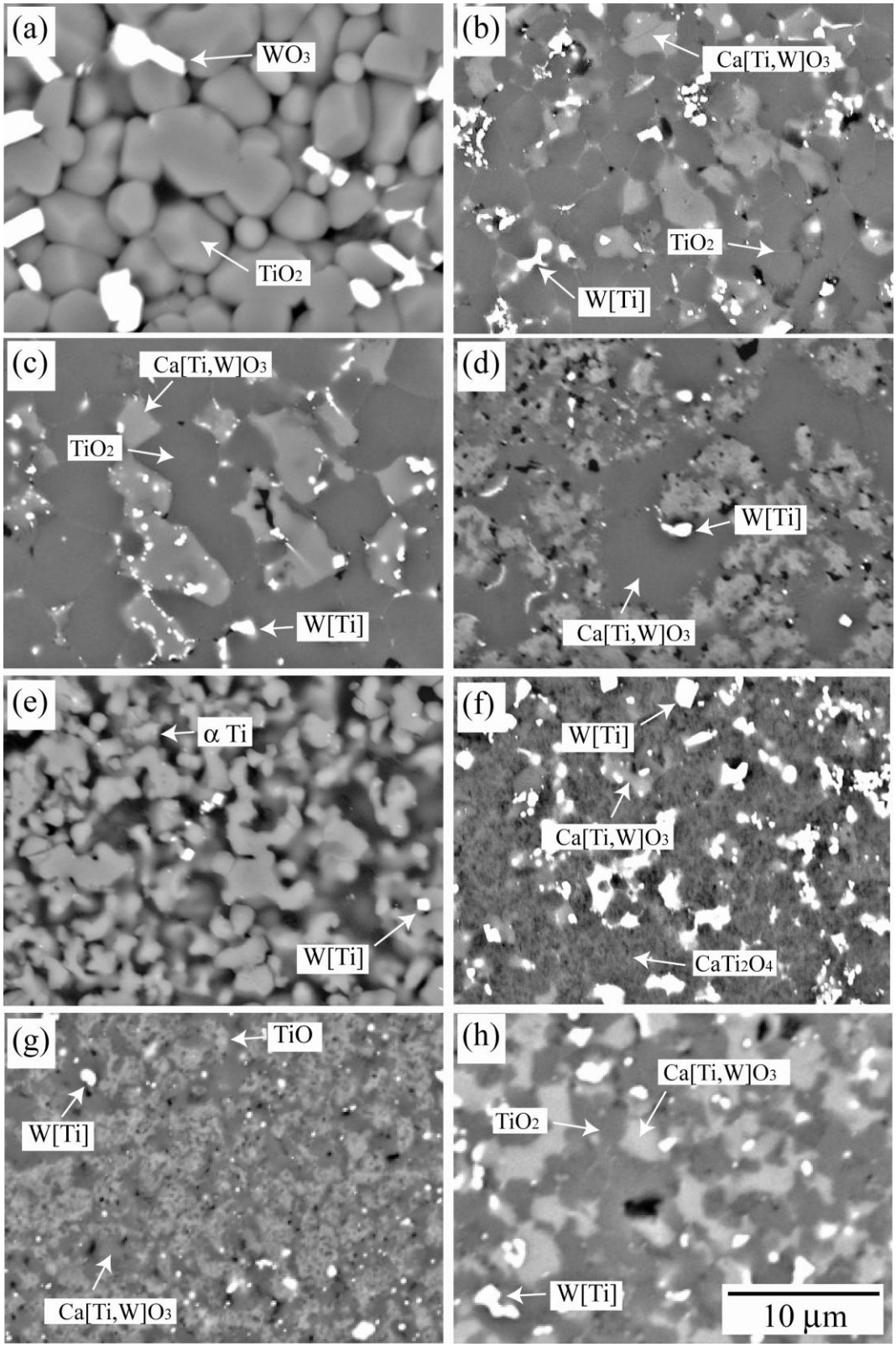

Figure 4 Back-scattered electron images of the (a) sintered precursor and partial reduced samples for (b) 600 s exposed, (c) 1 h core, (d) 1 h surface layer, (e) 3 h surface layer (Figure 7B), (f) 3 h intermediate layer – (Figure 8a) , (g) 3 h intermediate layer (Figure 8b), (h) 3 h core (Figure 7)

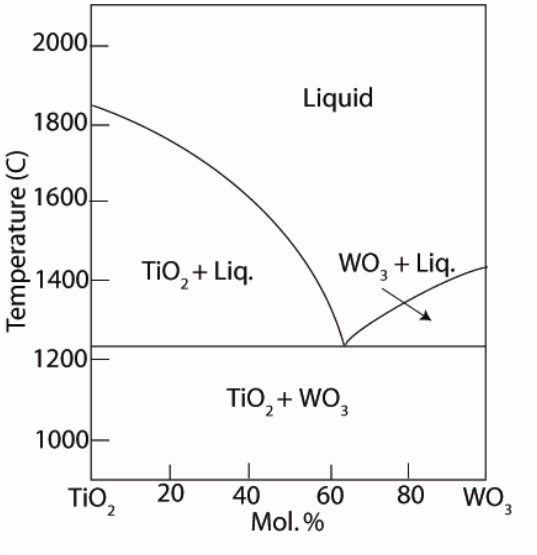

Figure 5 TiO_2-WO_3 equilibrium phase diagram (redrawn from Chang *et al.* [11])

The electrochemical reduction of metal oxides in $CaCl_2$ can be described by constructing electrochemical predominance diagrams described by Dring *et al.* [12]. Constructions for the Ca-Ti-O-Cl and Ca-W-O-Cl systems at 1173 K are shown in Figure 6. The potential for the oxidation of the electrolyte to form Cl_2 is defined as 0 mV. This is also known as the standard chlorine electrode (S.Cl.E) potential. The lower limit of the vertical axis is where the reduction of the electrolyte to unit activity calcium occurs, which is at -3231 mV for 1173 K. Thus, the range shown in Figure 6 represents the window in which the electrolyte is stable. The horizontal axis is defined as the negative log of the oxide activity in the electrolyte (pO^{2-}). The left hand side of the diagram, low pO^{2-}, is dominated by high-oxygen calcium titanate phases while the right hand side of the diagram, high pO^{2-}, is dominated by chloride phases.

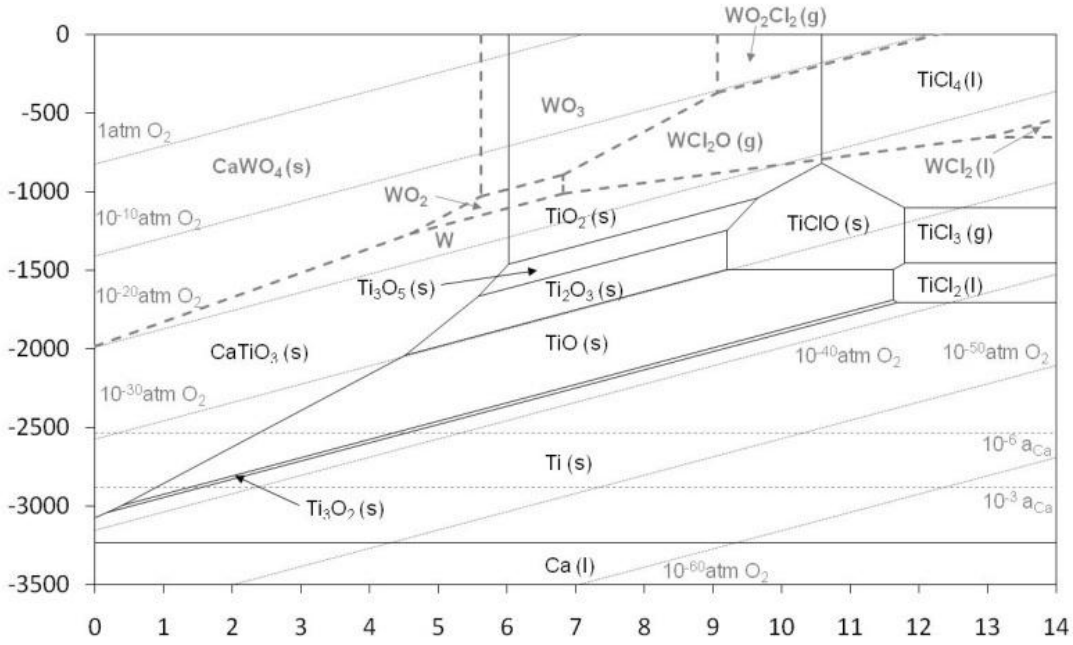

Figure 6 Overlaid electrochemical predominance diagram for the Ca-W-O-Cl and Ca-Ti-O-Cl systems

To understand what reactions take place when the sintered precursor is initially lowered into the electrolyte (i.e. while the sintered precursor is under steady state potential), a sample is exposed to the electrolyte for 600 s. The XRD trace for this sample (Figure 3b) reveals the presence of the phases W-Ti, TiO_2 and $CaTiO_3$. At the steady state potential (-1200 mV) the electrochemical predominance diagram predicts that the first reaction to take place is the electrochemical reduction of WO_3 to tungsten via reactions (1) and (2). This could occur as some current flows through the potentiostat, thus facilitating the electrochemical reaction. Alternatively, the titanium current collector, electrolyte and WO_3 could form a local galvanic cell which facilitates the reduction of WO_3 and oxidation of the titanium current collector. Another possible explanation for the reduction of WO_3 is the presence of calcium at less than unit activity, which acts as a reductant and chemically reduces the WO_3. The calcium could possibly be formed during the pre-electrolysis step where CaO and some of the electrolyte are decomposed. Figure 4b shows the presence of the three phases detected on the XRD trace. X-EDS reveals that the W-Ti particles have a composition of 96 wt. % W and 4 wt. % Ti. The titanium content of these particles is believed to be the result of a limited homogenisation of WO_2 with TiO_2 after reaction (1). The presence of $CaTiO_3$ in Figure 4b corresponds well with the presence of the W-Ti particles. This is most likely because, after the rapid reduction of WO_3, a large quantity of oxide ions is released into the electrolyte, which results in a significant rise in the local pO^{2-} of the electrolyte. This would result in a shift to the left hand side of the electrochemical predominance diagram (Figure 6), which would increase the likelihood of the chemical formation of $CaTiO_3$. The average composition of the $CaTiO_3$ is 31 wt. % O, 23 wt. % Ca, 33 wt. % Ti and 13 wt. % W, showing that tungsten has significant solid

solubility in $CaTiO_3$. This solid solution will be henceforth denoted as $Ca(Ti,W)O_3$. When incorporating tungsten into calcium titanate, tungsten ions replace the titanium ions in the lattice, thus providing additional free electrons. This will lead to a large increase in the electronic conductivity of this phase, which is believed to be beneficial for the reduction process.

$WO_3 + 2e^- = WO_2 + O_{2-}$ (1)

$C + 2O^{2-} = CO_2 + 2e^-$

$WO_2 + 4e^- = W + 2O_{2-}$ (2)

$C + 2O^{2-} = CO_2 + 4e^-$

After 1 h of reduction, the sample had two layers; the core of the sample and a ~150 µm thick surface layer. The morphology (Figure 4c) and phases detected by XRD (Figure 3C) are similar to that of the 600 s exposed sample (Figure 4b), indicating that after 1 h, little reduction within the core has taken place**.** The XRD trace for this sample (Figure 3c) reveals the presence of TiO, TiO_2, $CaTiO_3$ and W-Ti, therefore presumably the TiO is present in the surface layer. The BEI of the surface layer of the sample (Figure 4d) shows the presence of TiO and $CaTiO_3$. X-EDS analysis of these phases reveals that both phases had no tungsten content. Whilst this is expected for TiO, as tungsten has no 2+ valence state, it is anomalous for $CaTiO_3$. The author has previously hypothesised that the formation of oxychloride and chloride phases [13] is a mechanism by which metal oxides are lost to the electrolyte. While these losses are insignificant for the majority metal oxide, it can lead to significant changes in composition when a secondary metal oxide is present. As can be seen in the electrochemical predominance diagram phases (Figure 6), such as TiOCl, WCl_2O_2 and in particular WCl_2O, have large ranges of stability and exist at intermediary pO^{2-}. As these phases can form at less the unit activity (since they are soluble in the electrolyte) the stability fields for these particular phases can be further extended. The valence state of tungsten in $WOCl_2$ and WO_2Cl_2 are 4+ and 6+, respectively, thus, leading to losses of WO_2 and WO_3 from the sample via reactions (3) and (4). It is believed that this accounts for the tungsten depletion in the surface layer. Reactions (3) and (4) show that the formation of tungsten oxychlorides leads to a release of oxide ions, which lowers the pO^{2-} of the electrolyte leading to a shift left on the electrochemical predominance diagram and therefore, decreasing the likelihood of further oxychloride formation. It is interesting to note, that the $CaTiO_3$ at the surface layer, which is devoid of tungsten, and the $Ca(Ti,W)O_3$ in the core are not distinguishable by XRD.

$WO_2 + CaCl_2 = WCl_2O + CaO$ (3)

$WO_3 + CaCl_2 = WCl_2O_2 + CaO$ (4)

The XRD trace for the sample reduced for 3 h shows the presence TiO_2, $CaTiO_3$, TiO, W-Ti and α Ti. A layered structure can be observed after 3 h of reduction (Figure 7) with two thin surface layers and a core. However, using higher magnification imaging, the core can be resolved into two regions; the inner and outer core. The inner core of the sample, seen in Figure 4h, is similar to that seen in the core of the sample exposed to the electrolyte for 600s and reduced for 1 h (Figure 4b and Figure 4c), indicating that after 3 h of reduction the inner core remains largely unreduced. The outer core, shown in Figure 8, has a number of microstructural features. Upon closer inspection the features (Figure 4f) appear to be made of three phases which X-EDS indicates are $CaTiO_3$, $CaTi_2O_4$ and W-Ti. X-EDS revealed that the $CaTi_2O_4$ product had a low solubility for tungsten. Schwandt *et al.* [14] observed a comproportionation reaction in the presence of large concentrations of $CaTiO_3$ and TiO, which lead to the formation of $CaTi_2O_4$ via reaction (5). It is believed that a comproportionation between $Ca(Ti,W)O_3$ and TiO would lead to the formation of $CaTi_2O_4$ and W-Ti particles, which is the reason why increased quantities of W-Ti particles are observed in the $CaTi_2O_4$ regions (Figure 4f). The surrounding material (Figure 4g) appears to be a mixture of three phases, which X-EDS indicates are $CaTiO_3$, W-Ti and TiO. It is believed that the core material reduces in a similar way to that observed experimentally by Schwandt *et al.*, where it was observed that TiO_2 precursors reduces through the various lower oxides to titanium.

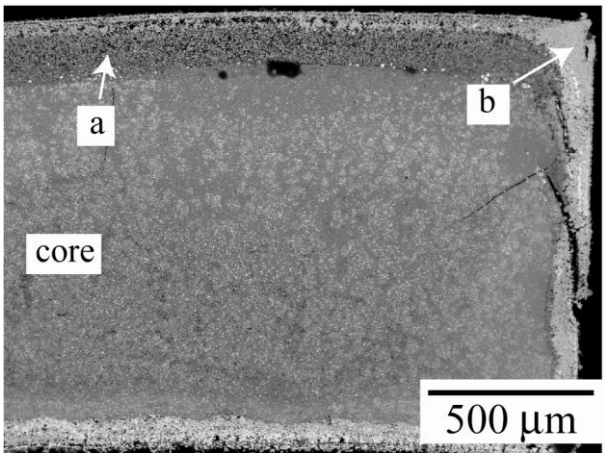

Figure 7 Sintered precursor reduced for 3 h; a) surface layer high porosity b) surface layer low porosity

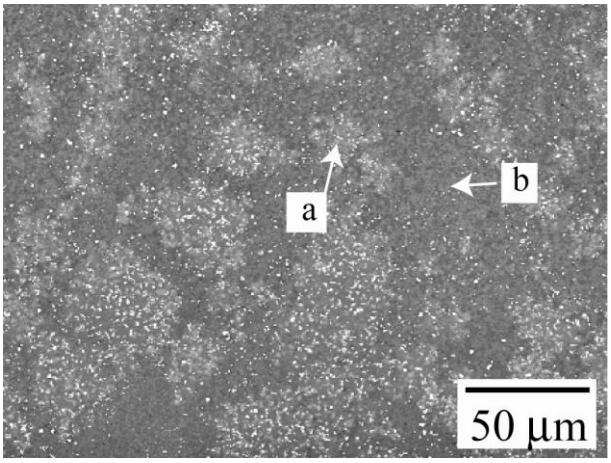

Figure 8 Sintered precursor reduced for 3 h; a) $CaTi_2O_4$ and W-Ti features b) $CaTiO_3$, W-Ti and TiO surrounding material

$$CaTiO_3 + TiO = CaTi_2O_4 \qquad (5)$$

After 1 h of reduction the surface contains a mixture of $CaTiO_3$ and TiO, which presumably transforms into $CaTi_2O_4$. The surface layer (both high and low porosity), seen in Figure 4e, which is a mixture of α Ti and W-Ti particles, is thought to be the result of the reduction of $CaTi_2O_4$ to Ti via reactions (6) and (7). One would expect that the W-Ti particles and product titanium particles would then begin to homogenise forming β Ti, as tungsten is an isomorphous β Ti stabiliser. However, the W-O-Ti equilibrium phase diagram (Figure 9) shows that the oxygen content in titanium directly affects the amount of tungsten that can be taken into solid solution. This is most likely due to the size of the substituting tungsten atom, which would impinge on the surrounding interstitial sites, in effect, making them unavailable to oxygen.

$$CaTi_2O_4 + 2e^- = 2TiO + CaO + O^{2-} \qquad (6)$$

$$TiO + 2e^- = Ti + O^{2-} \qquad (7)$$

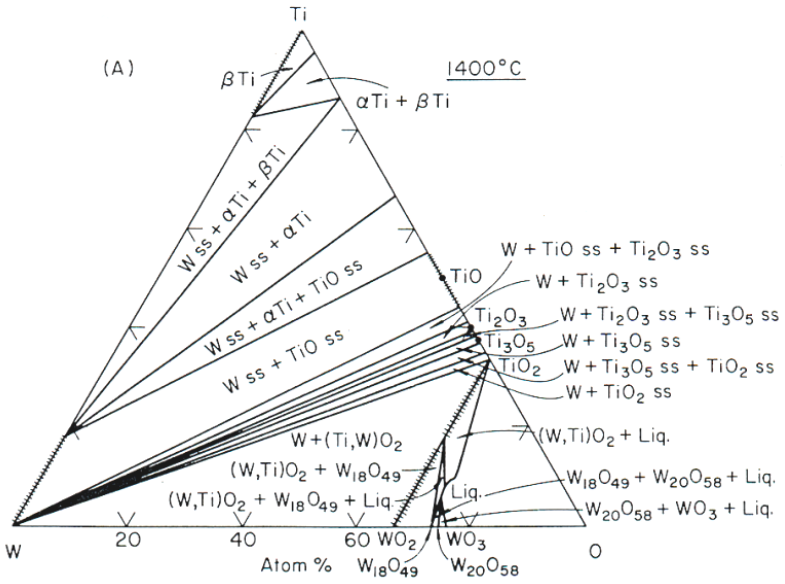

Figure 9 Ti-W-O equilibrium ternary phase diagram (redrawn from Chang *et al.* [15])

Once reduced for 6 h, two distinct regions can be identified by the naked eye, the ceramic core (Figure 10a) and the metal surface layer unchanged from the 3 h surface layer (Figure 4f). The average composition of α Ti in the surface layer was determined to be 13 wt. % O, 84 wt. % Ti and 3 wt. % W, though the individual W-Ti particle composition varied. The interface region (Figure 10b) between the core and surface layer interestingly shows the $CaTi_2O_4$ breaking up into particulate titanium. The XRD trace of the core (Figure 3e) reveals the presence of the phases $CaTi_2O_4$, $CaTiO_3$, W-Ti and α Ti. The BEI of the core and subsequent X-EDS analysis shows relatively small quantities of $Ca(Ti,W)O_3$, while the dominant phase appears to be $CaTi_2O_4$. This indicates that reaction (5) has proceeded further and is near to completion. The XRD trace of the surface layer of the 6 h reduction (Figure 3f) shows the presence of α Ti and W-Ti and is very similar to the surface layer of the 3 h reduction (Figure 4e).

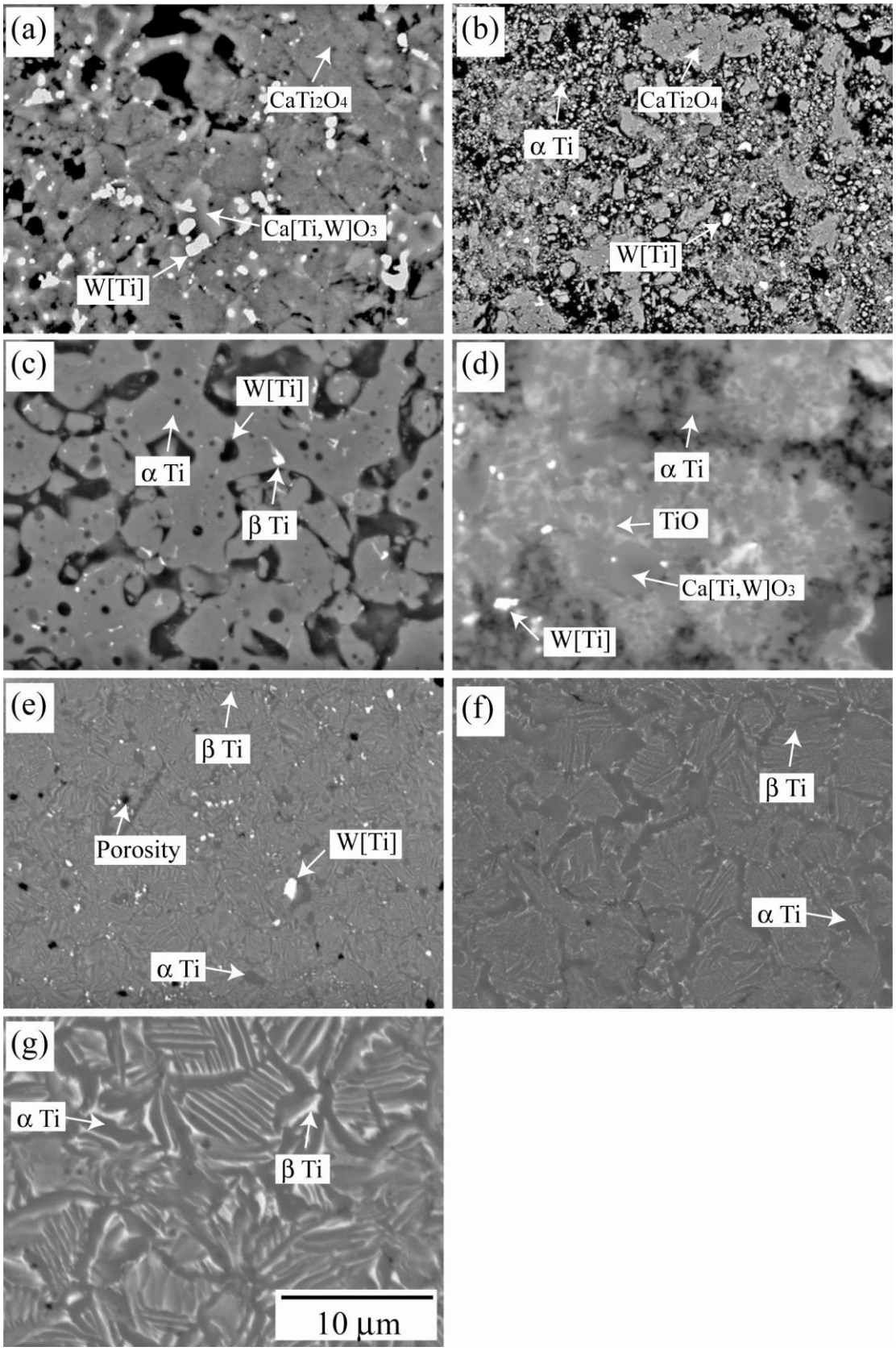

Figure 10 Back scattered images of partially reduced samples showing the (a) core region after 6 h, (b) interface region after 6 h, (c) surface layer after 9 h, (d) core region after 9 h, (e) 15 h, (f) 20 h and (g) 30 h

After 9 h of reduction the sample has two layers that could be resolved by eye; a ~700 μm surface layer and a core. The surface layer was determined, by XRD, to be a mixture of α and β Ti. The lack of W-Ti detected by XRD

suggests that homogenisation of the tungsten has taken place. Where as in the sample reduced for 3 h and 6 h, the surface layer was an agglomerate of titanium particles, the surface layer of the sample reduced for 9 h (Figure 10c) appears to have sintered and become a consolidated layer. This consolidation will, in effect, seal the core, resulting in a drastic reduction in electrolyte penetration. Thus, oxide ions ejected from further reduction within the core would be trapped and lower the local pO^{2-} of the electrolyte. The electrochemical predominance diagram demonstrates that as the pO^{2-} is lowered, the potential required to reduce a metal oxide becomes more negative, thus unfavourably impacting further reduction of the unreduced core.

Previous samples (1 h, 3 h and 6 h) appear to have a reduction front proceeding from the surface inward, which results in the formation of layers. However, the core of the sample reduced for 9 h appears to be reducing as a whole. The major phase within the core after 6 h of reduction was $CaTi_2O_4$ (Figure 10a). After 9 h, the BEI (Figure 10d) shows it consists of $CaTiO_3$ and a small volume fraction of TiO features surrounded by titanium particles. It is thought that this occurs as some of the $CaTi_2O_4$ acts as a solid electrolyte, i.e. transporting oxide ions from the reducing metal oxide to the entrapped $CaCl_2$. The local pO^{2-} of the electrolyte continues to decrease and it is believed that at eventually the flux of oxide ions entering the $CaTi_2O_4$ becomes greater than that leaving. This is achieved by filling the oxygen vacancies within $CaTi_2O_4$. This continues until $CaTi_2O_4$ saturates, at which point a dissociation of $CaTi_2O_4$ to $CaTiO_3$ and TiO occurs via reaction (8). The product $CaTiO_3$ can then accept more oxygen ions, thus facilitating the reduction of the surrounding material.

$$CaTi_2O_4 = CaTiO_3 + TiO \qquad (8)$$

After 15 h of reduction, the XRD trace reveals the presence of the phases W-Ti, α Ti and β Ti. Figure 10e shows that the density of W-Ti particles varies widely, with relatively high densities observed in the centre of the sample and low densities observed at the extremities of the sample. This effect, as described earlier, is likely due to the difference in oxygen contents of the reduced titanium. X-EDS analysis showed that the titanium within the core had several weight percent more oxygen than the extremities. Other than the W-Ti particles, the titanium matrix material is typical of that predicted by the Ti-W equilibrium phase diagram (Figure 11), which suggests that at the reduction temperature, the microstructure of a fully deoxidated Ti-10W alloy would be a fully β Ti solid solution. Upon equilibrium cooling, α Ti would nucleate at the grain boundaries, the most thermodynamically favourable sites for transformation. The α Ti formed would have a relatively low tungsten content (approximately 1-2 wt. % W), thus as more α Ti is formed, the remaining β Ti becomes increasingly tungsten rich. Eventually the sample

would reach 740°C and the remaining material would undergo the eutectic transformation. The microstructure seen in Figure 10e indicates that this is an accurate assessment.

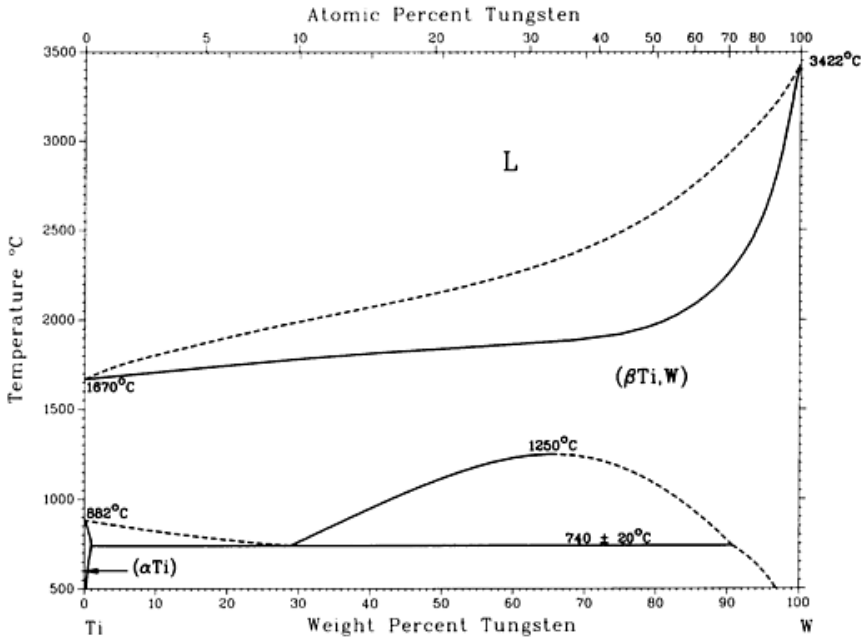

Figure 11 Ti-W equilibrium binary phase diagram (redrawn from Murray [16])

The samples reduced for 20 h (Figure 10f) and 30 h (Figure 10g) both exhibit typical furnace cooled structures with little or no residual W-Ti particles. This indicates that the titanium within the samples has been deoxidated to below 3 wt. % O, where all the remaining W-Ti particles have dissolved into the surrounding titanium. This is further confirmed by XRD analysis, which shows the presence of α Ti, β Ti and no W-Ti. The samples reduced for 20 h and 30 h were determined to have oxygen content of 0.6 wt. % and 0.4 wt. % respectively. An average grain size of 5 and 7 μm is observed in the samples reduced for 20 h and 30 h, respectively.

Conclusions

TiO_2-WO_3 precursors were formed by sintering TiO_2 and WO_3 powders together. Precursors sintered in argon were blue / purple in colour, which indicates the majority of the tungsten trioxide exists as W_5O_{14} and W_4O_{11} stoichiometries. The precursors sintered in air were yellow in colour, indicating the presence of the stoichiometric WO_3 phase. As the conductivity of the tungsten oxide Magnéli phases is greater thanWO_3, the former were preferred. Thus, all precursors were prepared by sintering under argon.

Ti-10W was successfully formed by electrochemically reducing mixed TiO_2-WO_3 sintered precursors. It was found that the reduction initiated with a rapid reduction of WO_3 to W-Ti via reactions (1) and (2). The presence of titanium in the W-Ti particles is most likely due to a homogenisation between TiO_2 and WO_2 post reaction (1). The

rapid reduction of WO_3 leads to a significant release of oxide ions which significantly lowers the local pO^{2-} of the electrolyte, and thus, favours the formation of $Ca(Ti,W)O_3$. This phase is believed to be the main route by which tungsten homogenisation occurs during reduction. Between 1 h and 3h, the sintered precursor consists of quantities of $Ca(Ti,W)O_3$ and TiO, which undergo a comproportionation reaction to form $CaTi_2O_4$ and W-Ti. After this reaction, fine W-Ti particles are homogenously distributed throughout the precursor. The $CaTi_2O_4$ then proceeds to reduces to titanium, via reactions (6) and (7).

During the reduction of $CaTi_2O_4$ described above, the formation of a thick consolidated surface layer occurs. This layer is observed at 9 h of reduction, at this stage in reduction further electrolyte penetration does not occur. Thus, as reduction of metal oxides within the sealed core proceed, oxide ions are ejected into the entrapped electrolyte resulting in a lowering of the local pO^{2-}. It is believed that in conjunction with the electrolyte the remaining $CaTi_2O_4$ begins to act as an oxide sink for the surrounding material; accepting oxide ions by filling oxygen vacancies within the lattice. Eventually it is thought that the $CaTi_2O_4$ would saturate and disproportionate into TiO and $CaTiO_3$. The $CaTiO_3$ product could then accept more oxide ions facilitating further reduction in the surrounding material.

The situation described above is thought to continue until the consolidated metallic layer sinters sufficiently for the formation of large cracks. These cracks allow fresh electrolyte to flow into the core, leading to an immediate increase in the local pO^{2-}. This would then facilitate the reduction of any remaining metal oxides within the core.

During the reduction process the only intermediatary metal oxide solid solution observed are $Ca(Ti, W)O_3$ and W-Ti. The presence of tungsten in solid solution within $CaTiO_3$ improves the electronic conductivity of the phase, which has a positive impact on the reduction process. However the formation of a conductive TiO network as observed by authors in the Ti-Mo system did not occur. Additionally, the formation of β Ti early in the reduction process as seen in the Ti-Mo system had a positive effect on the reduction process. Unfortunately, the formation of β Ti occurs late in the reduction of TiO_2-WO_3, as the presence of oxygen in solid solution with titanium detrimentally affects the solubility of tungsten in titanium. As such the electrochemical formation of Ti-Mo was more rapid than the formation of Ti-W under similar conditions.

Acknowledgements

The authors gratefully acknowledge the Defence Advanced Research Project Agency (DARPA), the Office of Naval Research and the Engineering and Physical Sciences Research Council (EPSRC) for their funding and support.

References

1. Kroll, W., Seventy-eighth general meeting, 1940: p. 35-47.
2. Crapper, D. R., Mclachlan, D. R., Farnell, B., Galin, H., Karlik, S., Eichhorn, G., De Boni, U., ed. Sarkar, B. 1993, New York: Raven Press. 209.
3. Steinemann, S. G., ed. G. Lu¨tjering, U.Z., and W. Bunk, eds. Vol. 2. 1985, Munich: Deutsche Gesellschaft Fur Metallkunde EV. 1373.
4. Choe, H., Abkowitz, S. M., Abkowitz, S., Dunand, D. C., Journal of Alloys and Compounds, 2005. **390**(1-2): p. 62-66.
5. Chen, G., Ma, M., Wang, D., Hu, X., Jin, X., Chem. Eur. J., 2006. **12**: p. 5075 – 5081.
6. Zhu, Y., Ma, M., Wang, D., Jiang, K., Hu, X., Jin, X., Chen, G., Chinese Science Bulletin, 2006. **51**(20): p. 2535-2540.
7. Bhagat, R., Jackson, M., Inman, D., Dashwood, R., J. Electrochem. Soc., 2007.
8. Dring, K., Bhagat, R., Jackson, M., Dashwood, R., Inman, D., J. Alloys Compd., 2006. **419**(1-2): p. 103-109.
9. Kuromoto, N. K., Simao, R. A., Soares, G. A., Materials Characterization, 2007. **58**(2): p. 114-121.
10. Wriedt, H. A., O (Oxygen) Binary Alloy Phase Diagrams, 1989.
11. Chang, L. L. Y., Scroger, M. G., Phillips, B., J. Less_Common Metals, 1967. **12**(1): p. 53.
12. Dring, K., Dashwood, R., Inman, D., J. Electrochem. Soc., 2005. **152**(10): p. D184-D190.
13. Bhagat, R., Jackson, M., Dashwood, R., 2007.
14. Schwandt, C., Fray, D. J., Electrochimica Acta, 2005. **51**(1): p. 66-76.
15. Chang, L. L. Y., Scroger, M. G., Phillips, B., J. Less-Common Metals, 1967. **12**(1): p. 54-55.
16. Murray, J. L., Wriedt, H. A., Bull. Alloy Phase Diagrams, 1987.